




Nanostructured CdO–ZnO composite thin films for sensing application

A. K. Sharma¹, S. S. Potdar^{2,*} , K. S. Pakhare³, U. M. Patil⁴, V. S. Patil⁵, and M. C. Naik⁶

¹ School of Physics, Shri Mata Vaishno Devi University, Kakryal, Katra, J&K 182320, India

² Department of Physics, Sanjeevan Engineering and Technology Institute, Panhala, Kolhapur, MS 416201, India

³ Department of Chemistry, Anandibai Raorane Arts, Commers and Science College, Dist-Sindhudurg, Vaibhavwadi, MS 416810, India

⁴ Centre for Interdisciplinary Research Studies, D.Y. Patil University, Kolhapur 416006, India

⁵ Department of Chemistry, Sanjeevan Engineering and Technology Institute, Panhala, Kolhapur, MS 416201, India

⁶ Smt. Kasturbai Walchanch College of Arts, Commerce and Sciences, Sangli, MS 416416, India

Received: 18 June 2020

Accepted: 4 October 2020

Published online:

16 October 2020

© Springer Science+Business Media, LLC, part of Springer Nature 2020

ABSTRACT

CdO–ZnO nanocomposites were synthesized by the facile SILAR method. In synthesis, 0.1 M Cd (NO₃)₂ and 0.1 M Zn (NO₃)₂ were used as sources of Cadmium and Zinc ions, respectively. The supersaturated solutions of Cd and Zn ions served as a cationic bath while 0.075 M NaOH as an anionic bath. To synthesize composite samples, the number of dipping is varied as 1:1, 1:2, and 1:3 concerning (CdO–ZnO). The XRD patterns of composite samples exhibit distinct peaks of ZnO and CdO, which clearly indicates the formation of CdO–ZnO nanocomposites in thin film form. The FE-SEM shows interlocked sheets with a thickness varies from ~ 30 nm to 300 nm for composites. EDAX mapping and XPS study, confirms that the obtained nanocomposite is actually composed of CdO and ZnO. The gas sensing behavior of CdO–ZnO is systematically investigated for 4 test gases under different operating temperatures and different gas concentrations. The maximum response of 52.04% is obtained for 24 ppm of Ethanol at a minimum operating temperature of 325 °C.

1 Introduction

Currently, a great deal of research is concentrated on the development of gas sensors for monitoring and detection of toxic gases. Numerous materials have been investigated for gas sensor applications. The development of fast and sensitive gas sensors with

small cross-sensitivity is the subject of intense research in the field of nanoscience and nanotechnology. However, developments in nanotechnology create a window for the synthesis of unique classes of nanostructured materials with enhanced gas sensing properties. The metal oxide semiconductors are attracted significant interest in the industrial and

Address correspondence to E-mail: sachinpotdar20@gmail.com

scientific field owing to their advantages, like small sizes, selectivity in the mixture of gases, enhanced sensitivities towards low concentrations of a wide range of gaseous chemical compounds, the possibility of on-line monitoring, and, due to cost-effectiveness [1] in comparison with traditional analytical instruments which faces many problems like the size of instruments, repeatability of results and also, difficulty in real-time analysis. Nanocrystalline oxides with controlled morphology as well as particle size lead to increasing demand in the field of gas sensing.

Different metal oxides such as SnO_2 , TiO_2 , WO_3 , ZnO , CdO , etc. had been extensively studied as the gas sensing element. Zinc oxide and Cadmium oxide has proven its diverse usage as a sensing agent owing to their different properties. ZnO has a wide direct bandgap (3.3 eV) [2] and excitation binding energy (60 meV) [3]. Also, Cadmium oxide (CdO), shows low resistivity and high transmittance in the visible region is advantageous in several applications [4, 5]. Also, both of them in the thin/thick film forms find the applications in numerous fields including, solar cells, gas sensors, electro-catalysis, etc. [6–13]. Chemical composition controls on microstructure, morphology, etc and can be tailored to get various physical and chemical properties. The selection of CdO and ZnO relies on the fact that, even though ZnO is excellent sensing material, its poor electrical conductivity limits its proficient application in gas sensors. On the other hand, CdO is a low resistive material, and thus it would reduce the resistance of the CdO/ZnO composite material. This would enable the easy detection of the resistance variation during the sensing measurement and the rapid electron transportation between the electrodes of the sensor [14]. Also, CdO is an n-type semiconductor with a large number of native oxygen vacancies [15, 16]. This property would be helpful to the adsorption of oxygen molecules on the surface of the CdO/ZnO composite, and the increase in the amount of surface chemisorbed oxygen should be advantageous to the surface reaction activity/kinetics and thereby improved sensing properties [17]. Several nanocomposites were prepared and studied for various applications such as $\text{ZnO}-\text{CuO}$ [18, 19], $\text{CdO}-\text{ZnO}$ [20], $\text{ZnO}-\text{SiO}_2$ [21], $\text{CdO}-\text{ZnO}$ [22], and $\text{PbO}-\text{ZnO}$ [23] for gas sensors, light-emitting diode, supercapacitor application, and photocatalytic activity, etc.

Several chemical methodologies were adopted to synthesize nanocomposite including sputtering [24],

sol-gel [25], hydrothermal [26, 27], Spray pyrolysis [28] methods, etc. Among the facile chemical deposition methods, the Successive ionic layer adsorption and reaction method (SILAR) is advantageous in terms of simple, inexpensive, facile, and rapid deposition techniques. The SILAR method is a modified method from chemical bath deposition (CBD), wherein the film is formed by a reaction from combined precursors in a well-ordered manner. Also, as reported by Shinde et al. [29], several chemical methods have the disadvantage of wastage of material because of the homogeneous reaction in the reaction bath. However, SILAR overcomes this disadvantage of wastage of material by avoiding precipitate formation in the solution. In the last few years, this method stands as one of the most important methods to deposit a large variety of materials over a large surface area [30–33]. The thickness of the film can be controlled also, morphology of film, grain size can be easily controllable by controlling over preparative parameters. This method is suited for different types of conducting and non-conducting substrates.

The present article focuses on the synthesis of $\text{CdO}-\text{ZnO}$ nanocomposite by the facile SILAR method. The influence of composition variation of CdO and ZnO on structural, morphological properties of $\text{CdO}-\text{ZnO}$ thin films are investigated employing X-ray diffraction (XRD), field-emission scanning electron microscopy (FE-SEM), Elemental dispersive X-ray analysis (EDAX) and X-ray photoelectron spectroscopy (XPS), etc., analysis. Furthermore, the gas sensing characteristic of the annealed samples was investigated for 4 test gases (TGs) viz: Ethanol, Hydrogen sulfide, Ammonia, and LPG. The rigorous study regarding sensitivity, selectivity at operating temperature is carried out. Also, Response and recovery were studied. The obtained results will help to amend and construct $\text{CdO}-\text{ZnO}$ electrodes based gas sensors.

2 Experimental

2.1 Chemicals used

Zinc Nitrate [$\text{Zn}(\text{NO}_3)_2$], Cadmium Nitrate [$\text{Cd}(\text{NO}_3)_2$], Sodium Hydroxide (NaOH), Liq. Ammonia etc., all chemicals are of analytical grade and used

without further purification. All the chemicals were purchased from Alfa Aesar chemicals.

2.2 Preparation of CdO–ZnO thin films

The CdO–ZnO nanocomposite was synthesized by successive ionic layer adsorption and reaction (SILAR) method. In this work glass microslides manufactured by 'Blue Star' with dimensions 75 mm × 25 mm × 1.35 mm were used as substrate. Initially, glass substrates were carefully washed with distilled water and soap solution. Subsequently, the glass substrates were heated in chromic acid (80–100 °C) for 1 h and kept in it for 5 h. Finally, films were washed with double distilled water and ultrasonically cleaned for 15 min at room temperature. Afterward, 0.1 M Zinc nitrate [Zn(NO₃)₂] and 0.1 M Cadmium nitrate [Cd(NO₃)₂] baths supersaturated with liquor ammonia were used as cationic baths. The NaOH (0.075 M) solution was used as an anionic bath for rapid reaction with adsorbed cations. To remove loosely held molecules present on the substrate of the newly adsorbed layer of ions, a distilled water bath was used as a rinsing bath. For the deposition of the films, the adsorption period was kept for the 30 s in a zinc bath and 20 s in a cadmium bath. The reaction period of the 20 s was kept for NaOH bath. Furthermore, successive dipping of cleaned glass substrates in cationic and anionic bath separated by rinsing bath was carried out for the deposition of thin films. Similarly, by changing the dipping sequence of the film in the CdO and ZnO bath, three samples were synthesized with stoichiometry as 1:1, 1:2, and 1:3 concerning (CdO–ZnO), respectively. In this method, the material deposition rate was very slow at the initial stage, after the 20 cycle increases rapidly up to 80 cycles. All five samples were synthesized and named pure CdO (SC), pure ZnO (SZ), and CdO–ZnO nanocomposite S1, S2, and S3 in the stoichiometric dipping of 1:1, 1:2, and 1:3 cycles, respectively. Furthermore, to remove hydroxyl species with structural water from films and convert them into respective oxides, the as-prepared samples were heat-treated at 450 °C for 2 h. Accordingly, a simple synthetic approach, the facile SILAR method is uniquely advantageous in terms of large-area deposition of material over different kinds of substrates.

The structures and morphologies of the electrode materials were characterized by XRD, XPS, and FE-

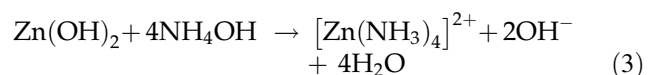
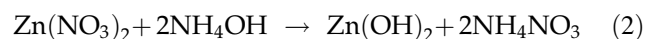
SEM measurements. The X-ray diffraction (XRD) pattern was carried out on a Rigaku Ultima IV diffractometer. X-ray photoelectron spectroscopy (XPS) measurements were carried out on a Thermo scientific K-alpha (Thermo Fisher Scientific, UK) using Al K α radiation. The morphology of the electrode materials was measured by field-emission scanning electron microscopy (FE-SEM, JSM-7001F, JEOL). The gas sensing properties of the CdO–ZnO films were studied in a Lab-made static gas sensor assembly wherein the Heater element is used to heat the sample at the desired temperature and Al–Cr thermocouple was used to sense the temperature of the samples. The gas inlet valve is there for injecting a known concentration of test gases. The silver paste is applied to the sample (1 cm × 1 cm) for providing electrical contacts. The electrical resistance of a CdO–ZnO film in the air (R_a) and in the presence of TGs (R_g) was measured to evaluate the gas sensing (S) defined in the literature [34] and given as:

$$\% \text{Sensitivity} = \frac{R_a - R_g}{R_a} \times 100 \quad (1)$$

3 Result and discussion

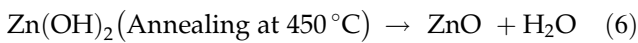
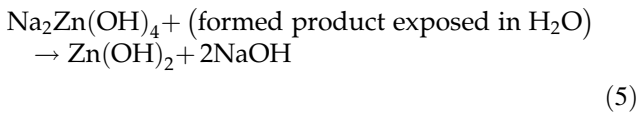
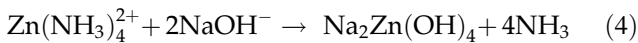
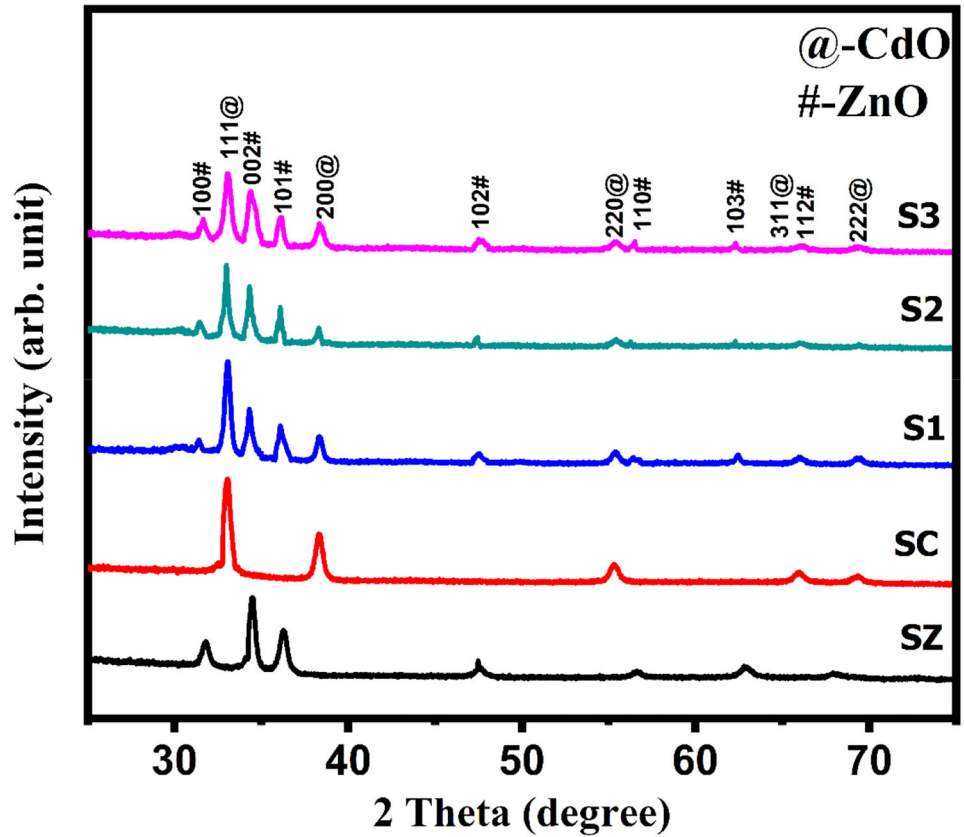
3.1 Thin film formation and structural studies (XRD)

The mechanism of ZnO film formation by SILAR method can be explained as follows. In the present case, the first precursor alkaline zinc nitrate solution is complexed with ammonia solution to obtain precipitate of zinc hydroxide. Ammonium nitrate is also obtained as byproduct. But in the presence of excess ammonia solution, the precipitate of tetraaminezinc (II) complex is formed and these reactions are represented as (Eqs. 2 and 3).

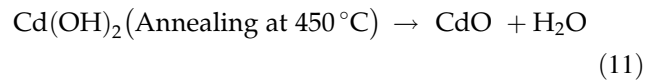
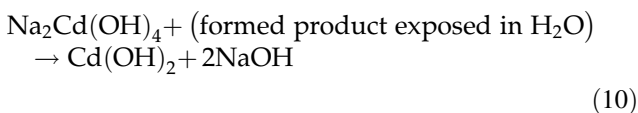
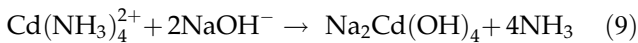
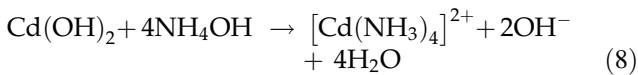
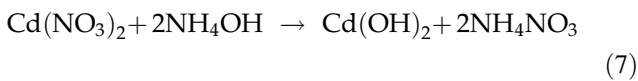


Now, in the presence of NaOH, NH₃ ligand gets replaced by OH[−] ions as shown in (Eqs. 4–6). Thus, the formed film surface was exposed in distilled water to remove sodium salt. Finally, one monolayer of Zn(OH)₂ / ZnO is deposited on the glass substrate. After annealing a final product of pure ZnO is formed.

Fig. 1 X-ray diffraction patterns of annealed CdO (SC), ZnO (SZ) and CdO–ZnO (S1, S2, S3) sample



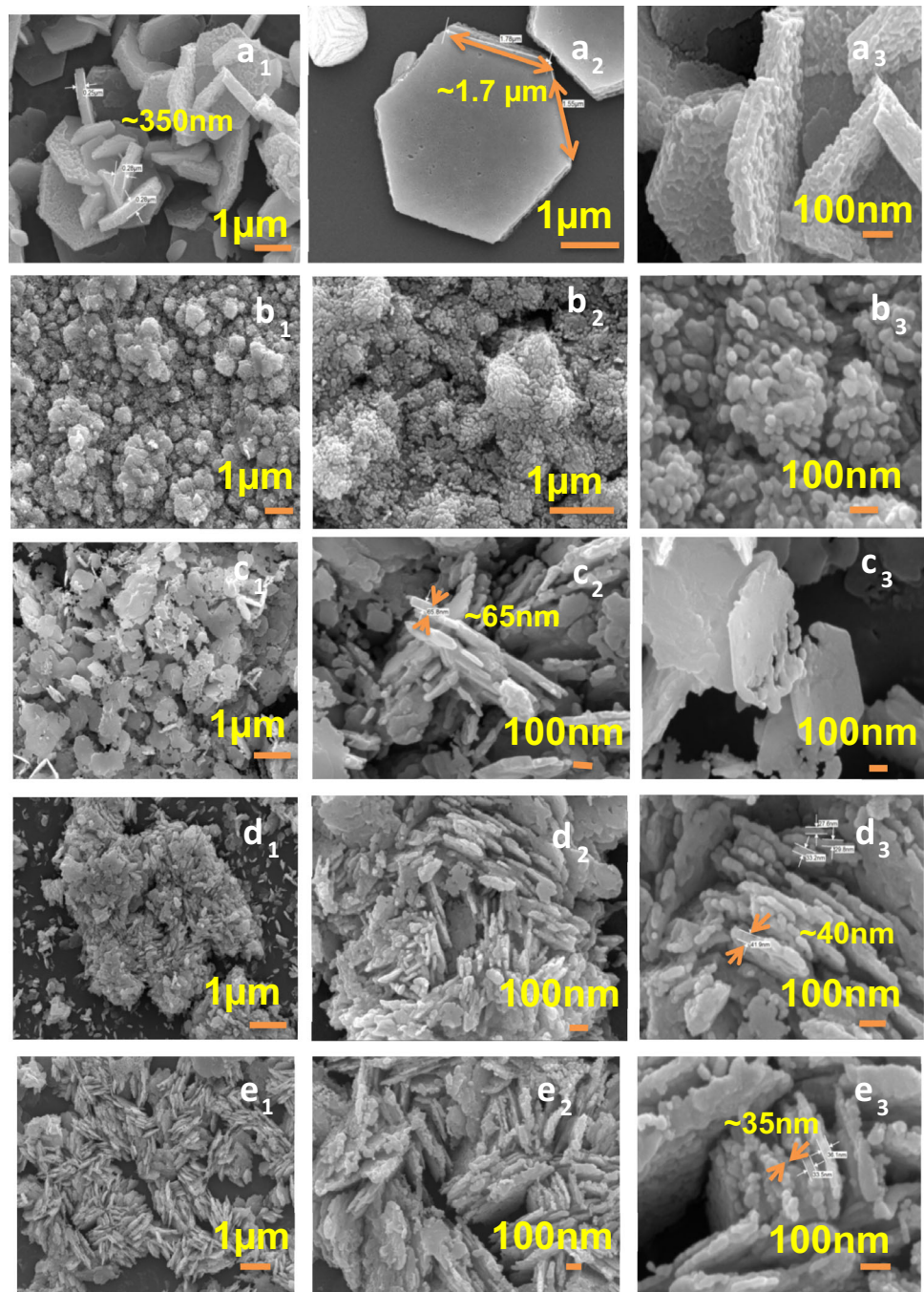
Similarly, deposition of Cd(OH)₂/CdO has been obtained by taking cadmium precursor and final product CdO is formed and it is given by the following equations.



Thus, by changing the dipping sequence of CdO and ZnO three samples were synthesized. The synthesized samples dipping stoichiometry were kept as 1:1, 1:2, and 1:3 concerning (CdO–ZnO).

The structural changes and identification of phases of the thin films obtained by SILAR method are investigated with the help of X-ray diffraction (XRD). The recorded XRD patterns, within diffraction angle (2θ) from 25° to 80°, for all the annealed thin films are shown in Fig. 1. Figure 1 reveals that all the samples are polycrystalline in nature. The XRD pattern obtained for the CdO–ZnO composite structure showed peaks from (111), (200), (220), and (311) planes corresponding to cubic CdO [marked as “@” (JCPDS no. 05-0640)]. Also, the peaks from planes (101), (102), (002), and (110) of ZnO were observed with little less intensity (marked as “#”). Also, the peak broadening is observed in composite samples might be due to an increase in structural disorder and the increase in density of point defects which affects

Fig. 2 Scanning electron micrographs of **a**_{1–3} CdO(SC), **b**_{1–3} ZnO(SZ), **c**_{1–3} CdO–ZnO1:1(S1), **d**_{1–3} CdO–ZnO1:2(S2), **e**_{1–3} CdO–ZnO1:3(S3)



crystallinity and grain boundary mobility which leads to FWHM broadening.

3.2 Scanning electron microscopy (SEM) and EDAX mapping

The surface and topographical study of annealed samples were investigated by Field effect Scanning Electron Microscopy (FE-SEM). The FE-SEM

micrographs of ZnO, CdO, and the composite CdO–ZnO films are shown in Fig. 2a–e at different magnifications. The FE-SEM micrographs (Fig. 2a1–3) show that the pure CdO is well-developed hexagonal petals with an average thickness of 320–360 nm with the length of hexagonal sides are about $\sim 1.7 \mu\text{m}$. However, bare ZnO thin films exhibit cauliflower-like morphology shown in Fig. 2b1, b2 and cauliflower consists of nanoparticles (Fig. 2b3). The FE-SEM

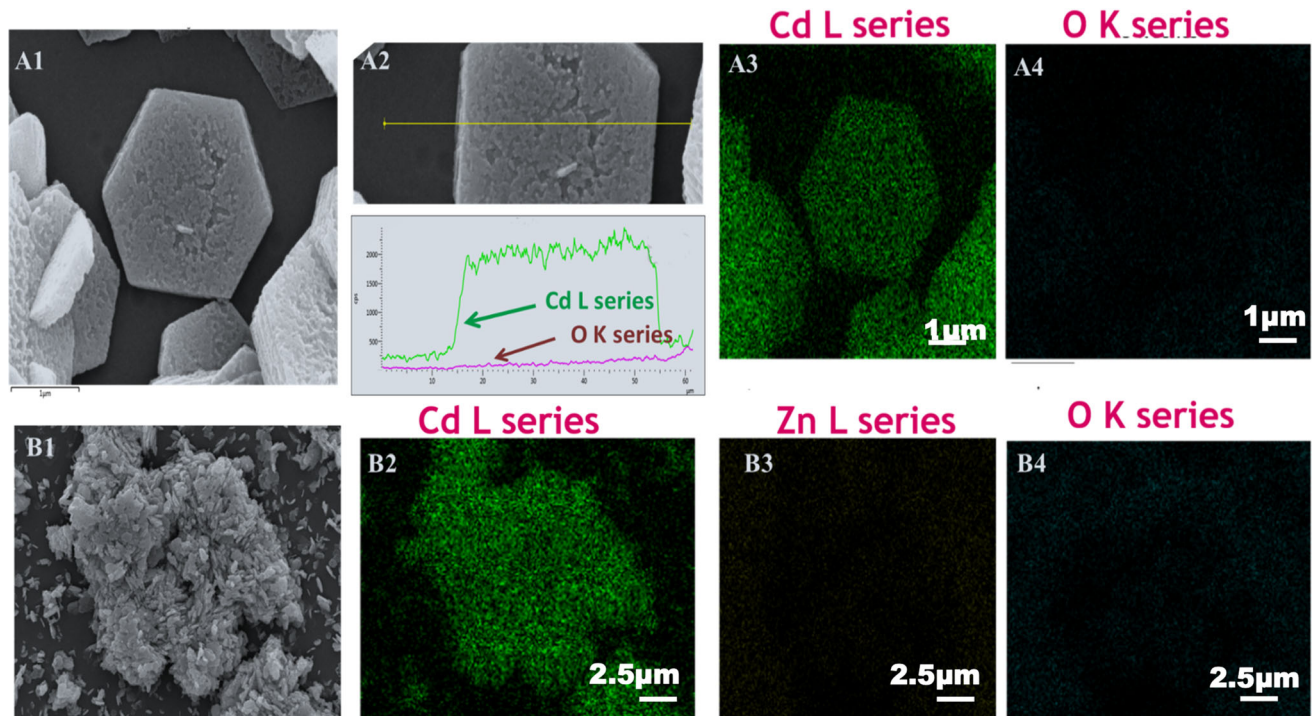


Fig. 3 a Elemental mapping of CdO (SC) Sample b Elemental mapping of CdO–ZnO (S3) Sample

images of CdO–ZnO compositions as 1:1, 1:2, and 1:3 (Cd:Zn) shown in Fig. 2c–e_{1–3} reveals a similar hexagonal petals-like structure. Interestingly, the size and width of hexagonal petals of CdO is reduced from 300 nm and found to be in the range of ~ 65 nm for CdO–ZnO with composition 1:1 (Fig. 2c1–3). The size of the petals of CdO–ZnO with composition 1:2 was further reduced and found to be ~ 40 nm (shown in Fig. 2d1–3). Furthermore, petals were found with a small size of about ~ 35 nm, as shown in Fig. 2e1–3f or the 1:3 compositions. The FE-SEM analysis reveals hexagonal petals of CdO reduce in size from ~ 350 to ~ 35 nm with increases in ZnO content.

To confirm the distribution of Zn, Cd, and O in the surface composite, elemental mapping, and line scanning is carried out. Figure 3A1 displays FE-SEM image of CdO, while Fig. 3A2–A4 show the line scanning and elemental mapping in different colors for Cd (green), O (blue). The EDS line scan of sample SC along the line is shown in Fig. 3A2 indicating enhanced Cd signals shown by bright spot which suggests that, the synthesized sample is highly Cd-rich. It is evident from Fig. 3A3–A4 that Cd is deposited at higher in density when compared to O. Elemental mapping of sample S3 shown in Fig. 3B1–

B4) reveals that Cd, Zn, and O are the main elements present in the sample. The Cd (green) deposited to a large extent in the central part of the substrate while Zn (yellow) and O (blue) deposited around the Cd.

3.3 X-ray photoelectron spectroscopy (XPS)

The surface chemical composition and chemical state of elements were studied by XPS analysis. Figure 4 shows the XPS spectrum of CdO–ZnO nanocomposite (sample S3). The peaks of Zn, Cd, and O can be clearly observed in the survey spectrum. From the survey spectrum Zn3d, Zn3p, Zn2p, Zn3s, Cd3d, Cd3p, Cd4d, and O1s levels were clearly seen. The energy scale is calibrated with the C1s peak of the carbon contamination at 284.08 eV. The Zn 2p XPS spectrum of sample S3 shows the doublet binding energies at 1044.68 and 1021.68 eV, which corresponding to Zn2p_{1/2} and Zn2p_{3/2}, respectively, which is in excellent agreement with the standard value of 22.97 eV. The first peak 1021.68 eV is attributed to Zn²⁺ ions in the oxygen-deficient ZnO environment [35]. Besides, the Zn 2p_{3/2} XPS peak is prominent. Thus, it can be affirmed, that Zn element exists mainly in the form of Zn²⁺ on the sample surfaces [36]. The Cd 3d spectrum of sample S3 presents the doublet binding energies at 412.08 eV and

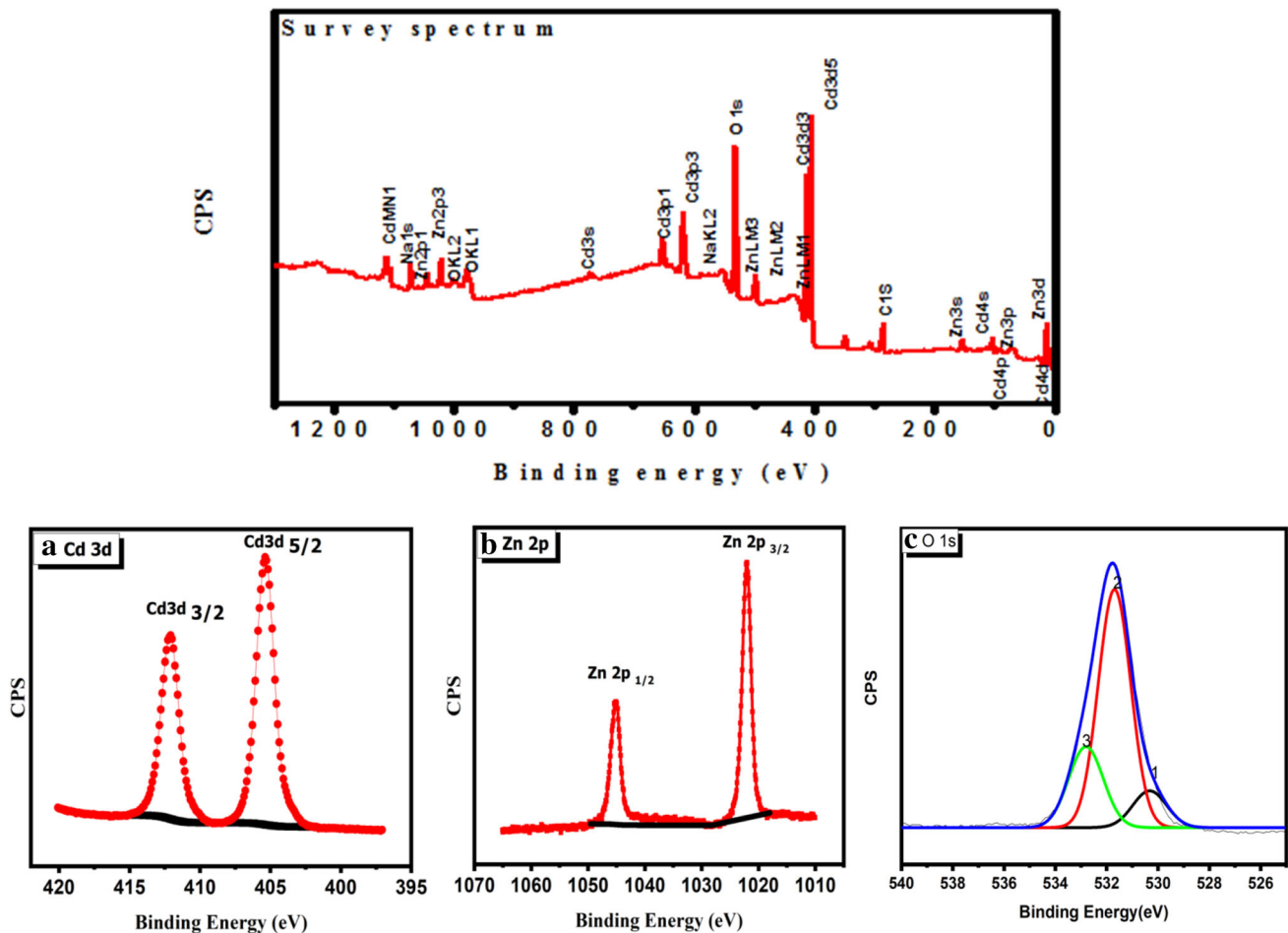


Fig. 4 XPS spectra of sample S3 **a** Cd3d **b** Zn 2p **c** O 1s

405.38 eV, which is corresponded to Cd 3d_{3/2} and Cd 3d_{5/2}, respectively. Moreover, the energy gap of 6.7 eV is observed between two peaks. The binding energy of Cd3d_{5/2} is attributed to the Cd²⁺ bonding state, which agrees well with the previous report [37]. Figure 4c illustrates the binding energies of the O 1s peak which were Gaussian-divided into O1, O2, and O3 bands. The curve was fitted to three distinctively components (denoted by 1, 2, and 3 in Fig. 4c). The peak 1 centered at 530.2 eV is attributed to O₂⁻ bonding with metal [38–40], i.e., Cd–O and Zn–O for the present study whereas the peak 2 situated at 531.65 eV is assigned to O₂⁻ state of oxygen defects or vacancies, supporting the formation of the non-stoichiometric ZnO. Finally, peaks 3 at 532.7 eV is connected with the contribution of surface OH group and possible Zn–Cd–O bond [41].

The occurrence of Zn peaks greater than 1021.5 eV and Cd peaks greater than 405 eV confirms the formation of the oxidized phase rather than the metal

phase. Normally, the metal phase always occurs at lower binding energy on account of the screening effect. The shifting of binding energy to a higher value is due to the shift of local charge density to the oxygen and reduction in screening effect. The peak shifting observed may be attributed to the charge redistribution process during chemical interaction.

3.4 Gas sensing properties

CdO and ZnO were extensively used as sensing elements owing to their interesting properties such as resistivity, optical band gap, etc.[42, 43]. Initially, the operating temperature of the sensor surface is determined as it is the most influencing parameter. For evaluation of sensing performance of CdO, ZnO, and CdO–ZnO nanocomposite to different test gases such as (NH₃, H₂S, C₂H₅OH, LPG), the films were exposed to 24 ppm of concentration of each gas at different operating temperature with the interval of

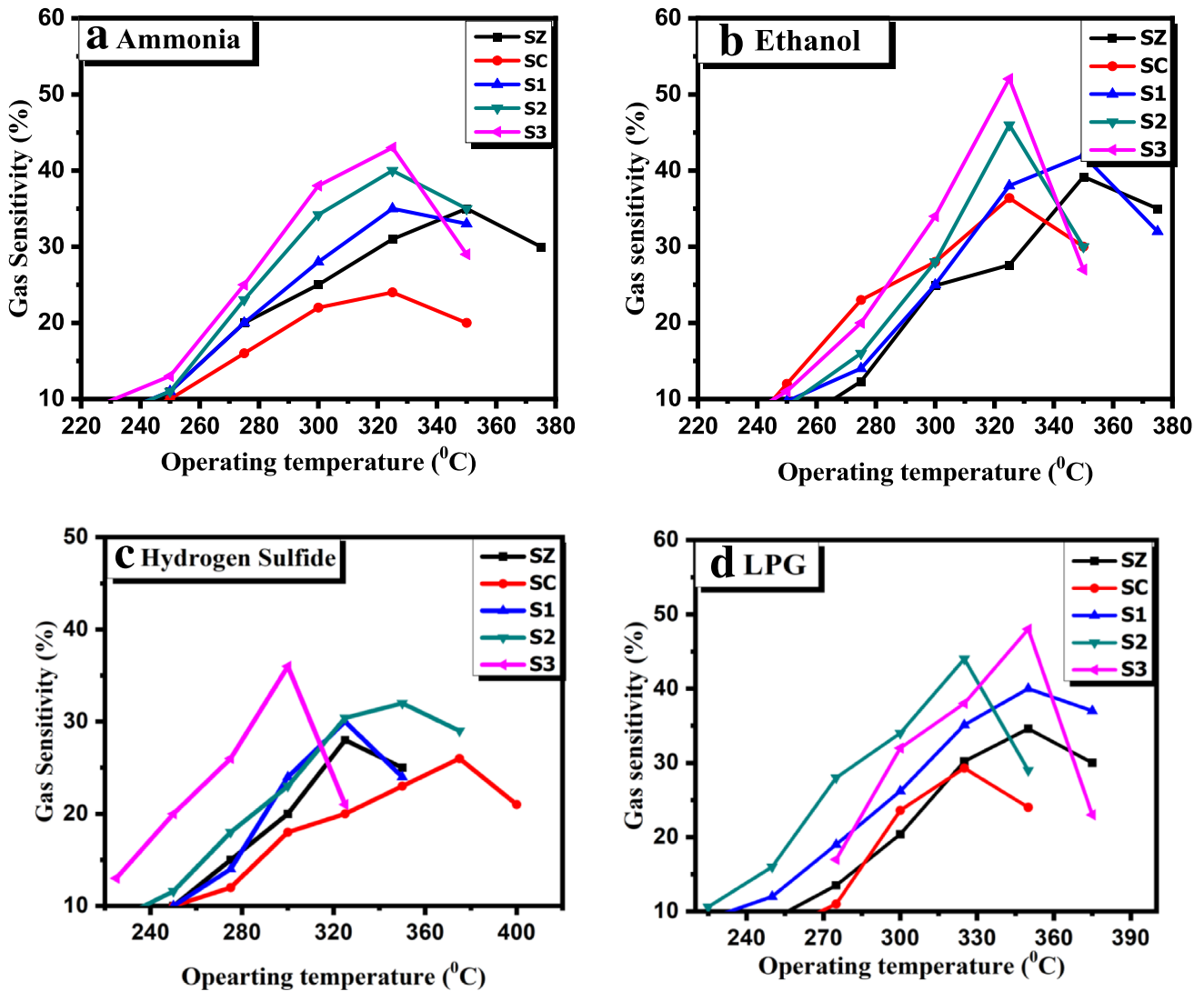


Fig. 5 Plot of Gas sensitivity as a function of operating temperature for different samples (SZ, SC, S1, S2, S3) for 24 ppm of **a** C₂H₅OH, **b** H₂S, **c** NH₃, **d** LPG

25 °C. The temperature at which the sensitivity is higher is the operating temperature of the sensor. Figure 5 shows the variation of gas sensitivity (%) with temperature for different sensors (sample SC, SZ, S1, S2 and S3) for 4 test gases viz: Ethanol (C₂H₅OH), Hydrogen Sulfide (H₂S), Ammonia (NH₃) and LPG. It is obvious from Fig. 5 that sensor S3 Shows superior gas sensing behavior over other sensors for all test gases even at lower operating temperatures and hence it is selected for further studies. Also, it is pointed out from Fig. 5 that CdO–ZnO composite shows better results in terms of sensitivity and also operating temperature over bare ZnO (SZ) as well as CdO (SC) for the different gases. Also, sample S3 is more sensitive towards Ethanol as

depicted in Fig. 6. The composite sensor S3 showed a 52.04% sensitivity to Ethanol at 325 °C operating temperature. Furthermore, CdO–ZnO sensor (S3) showed a response of 48% for the LPG at 350 °C and 36% for Hydrogen Sulfide at 300 °C. The sample S2 also showed comparable sensing for all gases. Further, even at the same concentration CdO–ZnO sensor exhibit higher sensitivity to Ethanol (about 52.04) than that of the Ammonia (NH₃) (~ 43), Hydrogen sulfide(H₂S) (~ 21), and LPG (~ 38) at an operating temperature of 325 °C as shown in Fig. 7a. The significant enhancement in sensitivity for composite sensor (S3) is observed in comparison with bare CdO or ZnO sensor under the same concentration at an operating temperature of 325 °C as given by Fig. 7b.

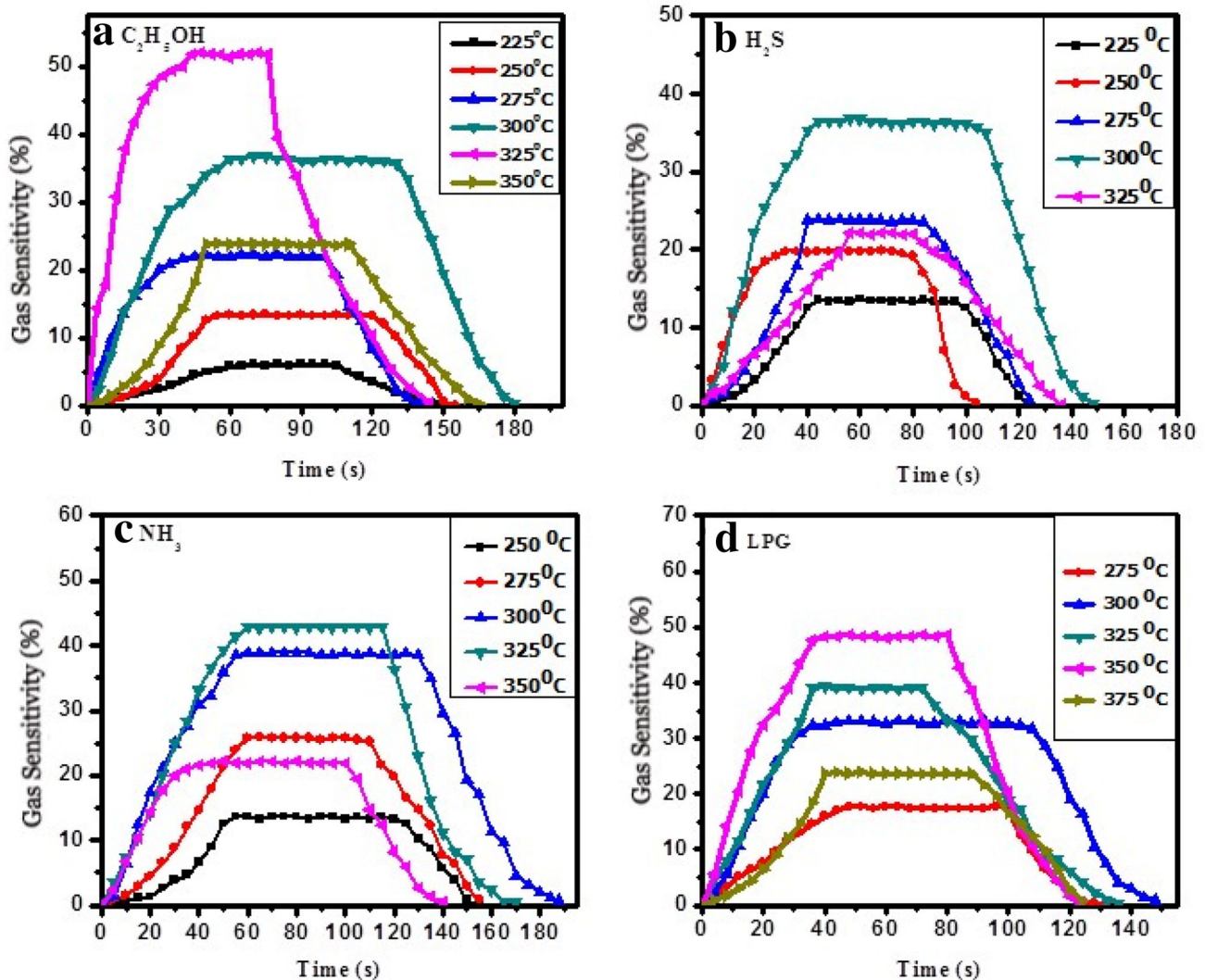


Fig. 6 Transient gas sensitivity of sample S3 at different operating temperature for 24 ppm of **a** C₂H₅OH, **b** H₂S, **c** NH₃, **d** LPG

Also, it is evident from Fig. 7c that composite sensor is more responsive (56 s) than pure ZnO and CdO sensors.

3.4.1 Sensing mechanism

The enhanced response of composite sensor in comparison with bare CdO and ZnO could be attributed to the heterojunction effect that occurred at intergrain boundaries between CdO–ZnO interface and morphological evolution due to composite formation. At intergrain boundaries between CdO and ZnO, electron transfer takes place since the difference between their Electron affinity, bandgap (3.37 eV for ZnO and 2.23 eV for CdO) and work function till Fermi level lies at equilibrium. So, in the area of heterocontact,

the enriched and depleted regions are formed as shown in Fig. 8. And thus edges of conduction as well as the valance band changes their energy by the amount given by the following equation [44]-

$$\Delta E = \frac{e^2}{2\epsilon_r} (n_{\text{CdO}}L_{\text{CdO}}^2 + n_{\text{ZnO}}L_{\text{ZnO}}^2) \quad (12)$$

L_{CdO} —length of the depleted layer in CdO side, n_{CdO} —Concentration of electrons in CdO, L_{ZnO} —length of the accumulated layer in ZnO side, n_{ZnO} —Concentration of electrons in ZnO, ϵ_r —relative permittivity of the material.

The development of this built-in potential hampers the flow of electrons, in other words, it acts as a resistor element in a series manner in composite nanosheets. Due to this, the significant change in

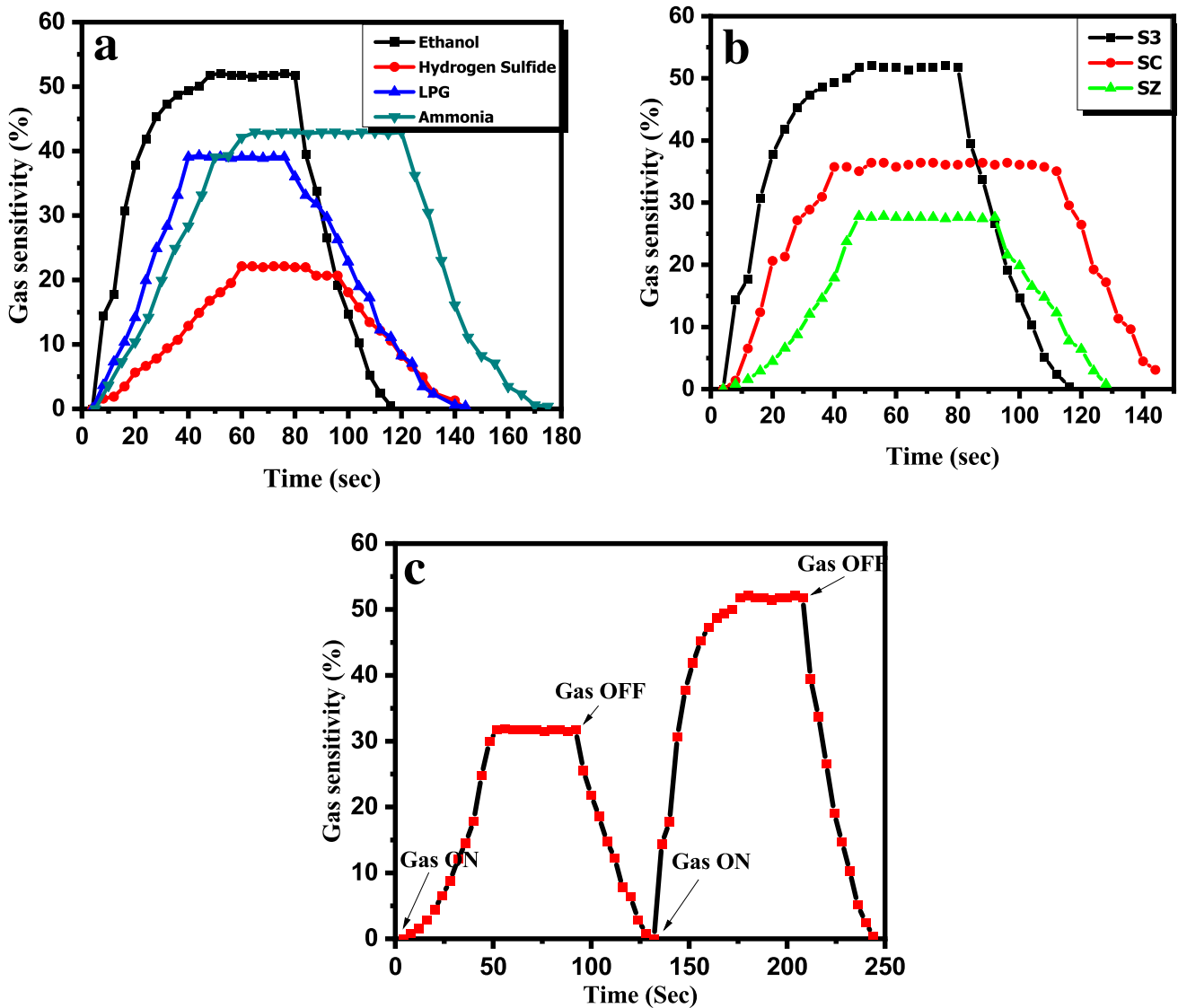


Fig. 7 **a** Transient gas sensitivity of sample S3 at 325 °C for 24 ppm of C₂H₅OH, H₂S, NH₃ and LPG, **b** Transient gas sensitivity of sample S3, SZ and SC at 325 °C for 24 ppm C₂H₅OH, **c** response and recovery of sample S3 at 325 °C for 24 ppm C₂H₅OH

resistance occurs during the elimination and re-creation of electrons by the adsorption and desorption of ethanol, respectively. And thus exhibiting superior ethanol sensing performance.

4 Conclusions

The CdO, ZnO and CdO–ZnO nanocomposite thin films have been successfully synthesized by the Successive ionic layer adsorption and reaction (SILAR) method. The XRD, SEM, and EDS mapping depicts that, the formation of polycrystalline, cauliflower-like morphology for ZnO while hexagonal

petals-like morphology for CdO. However, a nanocomposite of CdO–ZnO shows interlocked petal-like sheets with an average size of about ~ 65–35 nm. XPS study reveals that composite made up of CdO and ZnO. The maximum response of 52.04% for 24 ppm of Ethanol at an operating temperature of 325 °C is achieved for CdO–ZnO sample with the proportion as 1:3. The CdO–ZnO (S3) sensor is selective towards Ethanol against Ammonia, Hydrogen sulfide, and LPG. The heterojunction effect at intergrain boundaries and morphological evolution with the high surface area of CdO–ZnO (S3) exhibits high gas sensing response with selectivity towards Ethanol. Thus, the facile SILAR synthetic

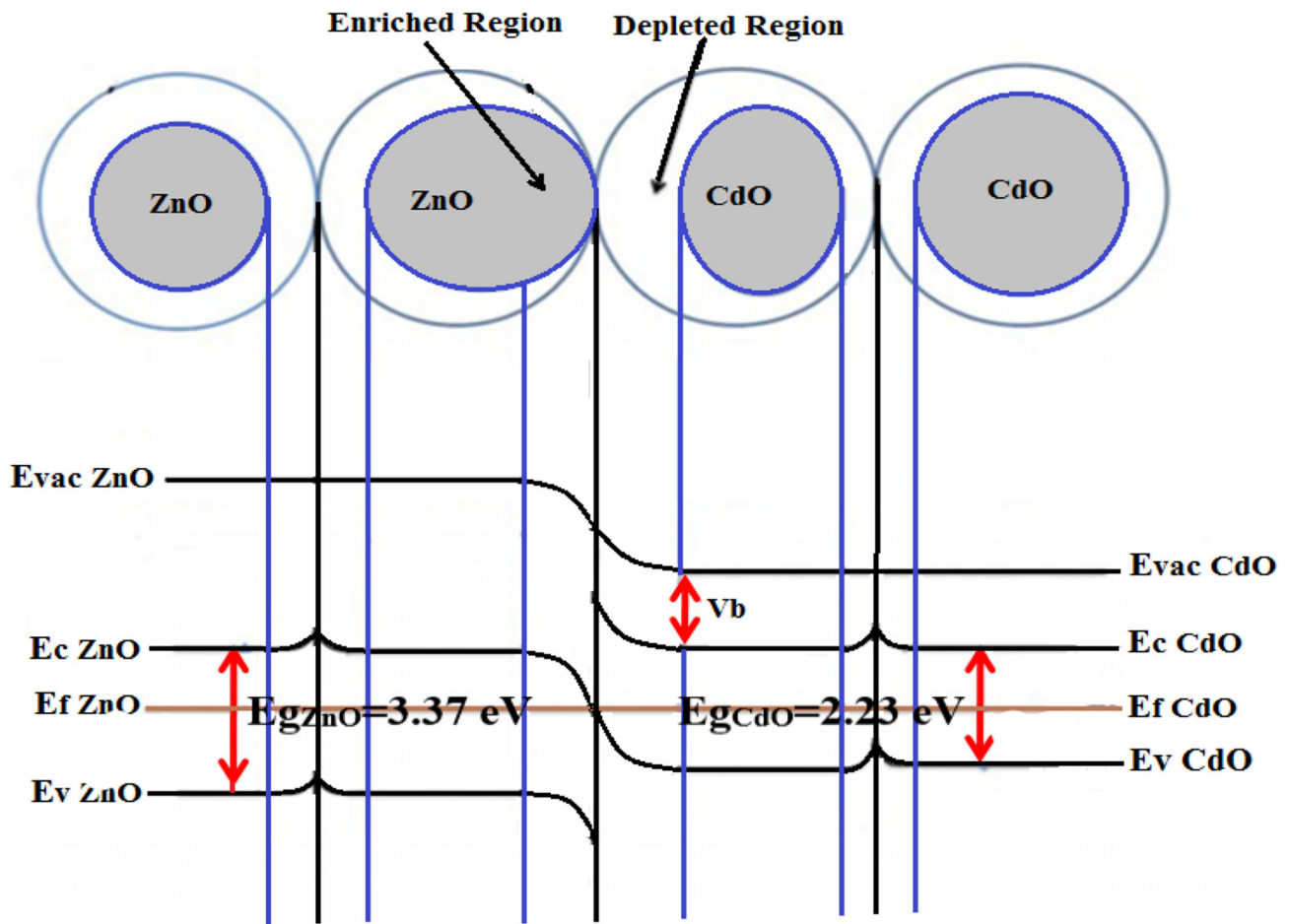


Fig. 8 Schematic diagram of band bending at heterocontact between CdO and ZnO

approach may provide a convenient route for the preparation of large scale CdO–ZnO thin films as an efficient electrode in high-performance gas sensing and open up the further scope in selective gas sensor device application.

Compliance with ethical standards

Conflict of interest There is no conflict of interest.

References

1. A. Mandeles, C. Christofides, *Chemistry and Technology of Solid State Gas Sensor Devices* (Wiley & Sons Inc, New York, 1993)
2. M.H. Huang, S. Mao, H. Feick, H. Yan, Y. Wu, H. Kind, E. Weber, R. Russo, P. Yang, Room-temperature ultraviolet nanowire nanolasers. *Science* **292**, 1897–1899 (2001)
3. A.I. Inamdar, S.H. Mujawar, P.S. Patil, The influences of complexing agents on growth of zinc oxide thin films from zinc acetate bath and associated kinetic parameters. *Int. J. Electrochem. Sci* **2**, 797–808 (2007)
4. M. Ocampo, A.M. Fernandez, P.J. Sebastian, Transparent conducting CdO films formed by chemical bath deposition. *Semicond. Sci. Technol.* **8**(5), 750–751 (1993). <https://doi.org/10.1088/0268-1242/8/5/024>
5. A.C. Nwanya, P.R. Deshmukh, R.U. Osuji, M. Maaza, C.D. Lokhande, F.I. Ezema, Synthesis, characterization and gas-sensing properties of SILAR deposited ZnO–CdO nanocomposite thin film. *Sensors and Actuators B: Chemical* **206**, 671–678 (2015). <https://doi.org/10.1016/j.snb.2014.09.111>
6. B. Sang, K. Dairiki, A. Yamada, M. Konagai, High-efficiency amorphous silicon solar cell with Zn as front contact. *Jap J. Appl. Phys.* **38**, 4983–4988 (1999)
7. R.S. Mane, H.M. Pathan, C.D. Lokhande, S.-H. Han, An effective use of nanocrystalline CdO thin films in dye-sensitized solar cells. *Sol. Energy* **80**(2), 185–190 (2006). <https://doi.org/10.1016/j.solener.2005.08.013>
8. V.R. Shinde, T.P. Gujar, C.D. Lokhande, LPG sensing properties of ZnO films prepared by spray pyrolysis method: effect

- of molarity of precursor solution. *Sensors and Actuators B Chemical* **120**(2), 551–559 (2007). <https://doi.org/10.1016/j.snb.2006.03.007>
9. R. Waghulade, P. Patil, R. Pasricha, Synthesis and LPG sensing properties of nano-sized cadmium oxide. *Talanta* **72**(2), 594–599 (2007). <https://doi.org/10.1016/j.talanta.2006.11.024>
 10. V.R. Shinde, T.P. Gujar, C.D. Lokhande, R.S. Mane, S.-H. Han, Use of chemically synthesized ZnO thin film as a liquefied petroleum gas sensor. *Mater. Sci. Eng., B* **137**(1–3), 119–125 (2007). <https://doi.org/10.1016/j.mseb.2006.11.008>
 11. M.S. Wagh, G.H. Jain, D.R. Patil, S.A. Patil, L.A. Patil, Modified zinc oxide thick film resistors as NH₃ gas sensor. *Sensors Actuators B Chem* **115**(1), 128–133 (2006). <https://doi.org/10.1016/j.snb.2005.08.030>
 12. A.Z. Sadek, S. Choo-pun, W. Wlodarski, S.J. Ippolito, K. Kalantar-zadeh, Characterization of ZnO nanobelt-based gas sensor for H₂, NO₂, and hydrocarbon sensing. *IEEE Sens. J.* **7**(6), 919–924 (2007). <https://doi.org/10.1109/jnsen.2007.895963>
 13. R.R. Salunkhe, D.S. Dhawale, U.M. Patil, C.D. Lokhande, Improved response of CdO nanorods towards liquefied petroleum gas (LPG): effect of Pd sensitization. *Sensors Actuators B Chem* **136**(1), 39–44 (2009). <https://doi.org/10.1016/j.snb.2008.10.048>
 14. G. Lu, L.E. Ocola, J. Chen, Room-temperature gas sensing based on electron transfer between discrete tin oxide nanocrystals and multiwalled carbon nanotubes. *Adv. Mater.* **21**(24), 2487–2491 (2009). <https://doi.org/10.1002/adma.200803536>
 15. A.S. Kamble, R.C. Pawar, N.L. Tarwal, L.D. More, P.S. Patil, Ethanol sensing properties of chemosynthesized CdO nanowires and nanowalls. *Mater. Lett.* **65**(10), 1488–1491 (2011). <https://doi.org/10.1016/j.matlet.2011.02.049>
 16. D.S. Raj, T. Krishnakumar, R. Jayaprakash, T. Prakash, G. Leonardi, G. Neri, CO sensing characteristics of hexagonal-shaped CdO nanostructures prepared by microwave irradiation. *Sensors and Actuators B Chemical* **171–172**, 853–859 (2012). <https://doi.org/10.1016/j.snb.2012.05.083>
 17. J. Su, X.X. Zou, Y.C. Zou, G.D. Li, P.P. Wang, J.S. Chen, Porous titania with heavily self-doped Ti³⁺ for Specific Sensing of CO at Room Temperature. *Inorg. Chem* **52**, 5924–5930 (2013)
 18. M. Bahu, K. Kumar, T. Bahu, CuO-ZnO Semiconductor gas sensor for ammonia at room temperature. *E. Devices* **14**, 1137–1141 (2012)
 19. Y. Hu, X. Zhou, Q. Han, Q. Cao, Y. Huang, Sensing properties of CuO/ZnO heterojunction gas sensors. *Mater. Sci. Eng. B* **99**, 41–43 (2003)
 20. H. Karami, Investigation of sol-gel synthesized CdO-ZnO nanocomposite for CO gas sensing. *Int. J. Electrochem. Sci* **5**, 720–730 (2010)
 21. P. Thiyagarajan, M. Kottaisamy, N. Rama, M.S.R. Rao, White light emitting diode synthesis using near ultraviolet light excitation on zinc oxide-silicon dioxide nanocomposite. *Scripta Mater.* **59**(7), 722–725 (2008). <https://doi.org/10.1016/j.scriptamat.2008.06.006>
 22. C.V. Reddy, B. Babu, J. Shim, Synthesis, optical properties and efficient photocatalytic activity of CdO/ZnO hybrid nanocomposite. *J. Phys. Chem. Solids* **112**, 20–28 (2018). <https://doi.org/10.1016/j.jpics.2017.09.003>
 23. H. Sivaram, D. Selvakumar, A. Alsalmeh, A. Alswieleh, R. Jayavel, Enhanced performance of PbO nanoparticles and PbO-CdO and PbO-ZnO nanocomposites for supercapacitor application. *J. Alloy. Compd.* **731**, 55–63 (2018). <https://doi.org/10.1016/j.jallcom.2017.10.025>
 24. B. Sharma, A. Sharma, M. Joshi, J. Ha-Myung, Sputtered SnO₂/ZnO heterostructures for improved NO₂ gas sensing properties. *Chemosensors* **8**(3), 67–67 (2020). <https://doi.org/10.3390/chemosensors8030067>
 25. J. Wang, Z. Chen, Y. Liu, C. Shek, C.M.L. Wu, J.K.L. Lai, Solar energy materials & solar cells heterojunctions and optical properties of ZnO/SnO₂ nanocomposites adorned with quantum dots. *Sol. Energy Mater. Sol. Cells* **128**, 254–259 (2014)
 26. C. Wang, X. Cheng, X. Zhou, P. Sun, X. Hu, K. Shimanoe, G. Lu, N. Yamazoe, Hierarchical α -Fe₂O₃/NiO composites with a hollow structure for a gas sensor. *ACS Appl. Mater. Interfaces.* **6**(15), 12031–12037 (2014). <https://doi.org/10.1021/am501063z>
 27. Y. Mingli, Y. Yao, F. Haibo, L. Shengzhong, WO₃-SnO₂ nanosheet composites: hydrothermal synthesis and gas sensing mechanism. *J. Alloys Compd* **736**, 322–331 (2018)
 28. T. Tharsika, M. Thanishaichelvan, A.S.M.A. Haseeb, S.A. Akbar, Highly sensitive and selective ethanol sensor based on ZnO nanorod on SnO₂ thin film fabricated by spray pyrolysis. *Frontiers Mater.* **6**, 122–122 (2019). <https://doi.org/10.3389/fmats.2019.00122>
 29. V.R. Shinde, T.P. Gujar, C.D. Lokhande, Studies on growth of ZnO thin films by a novel chemical method. *Sol. Energy Mater. Sol. Cells* **91**(12), 1055–1061 (2007). <https://doi.org/10.1016/j.solmat.2007.02.017>
 30. S.S. Kale, R.S. Mane, H.M. Pathan, A.V. Shaikh, O.-S. Joo, S.-H. Han, Preparation and characterization of ZnTe thin films by SILAR method. *Appl. Surf. Sci.* **253**(9), 4335–4337 (2007). <https://doi.org/10.1016/j.apsusc.2006.09.043>
 31. Y.F. Nicolau, M. Dupuy, M. Brunel, ZnS, CdS, and Zn_{1-x}S × S thin films deposited by the successive ionic layer

- adsorption and reaction process. *J. Electrochem. Soc.* **137**(9), 2915–2924 (1990). <https://doi.org/10.1149/1.2087099>
32. S.D. Sartale, C.D. Lokhande, Attractive microwave-absorbing properties of $\text{La}_1 \times \text{Sr} \times \text{MnO}_3$ manganite powders. *Mater. Chem. Phys.* **72**(1), 101–104 (2001)
33. H.M. Pathan, S.S. Kale, C.D. Lokhande, S.-H. Han, O.-S. Joo, Preparation and characterization of amorphous manganese sulfide thin films by SILAR method. *Mater. Res. Bull.* **42**(8), 1565–1569 (2007). <https://doi.org/10.1016/j.materresbull.2006.11.017>
34. M.S. Wagh, L.A. Patil, T. Seth, D.P. Amalnerkar, Surface cupricated SnO_2 -ZnO thick films as a H_2S gas sensor. *Mater. Chem. Phys.* **84**(2–3), 228–233 (2004). [https://doi.org/10.1016/s0254-0584\(03\)00232-3](https://doi.org/10.1016/s0254-0584(03)00232-3)
35. S.Y. Huang, Q.J. Cheng, S. Xu, D.Y. Wei, H.P. Zhou, J.D. Long, I. Levchenko, K. Ostrikov, Self-organized ZnO nanodot arrays: effective control using SiN_x interlayers and low-temperature plasmas. *J. Appl. Phys.* **111**(3), 036101–036101 (2012). <https://doi.org/10.1063/1.3673593>
36. J. Liqiang, W. Dejun, W. Baiqi, L. Shudan, X. Baifu, F. Honggang, S. Jiazhong, Effects of noble metal modification on surface oxygen composition, charge separation and photocatalytic activity of ZnO nanoparticles. *J. Mol. Catal. A Chem.* **244**(1–2), 193–200 (2006). <https://doi.org/10.1016/j.molcata.2005.09.020>
37. V. Stambouli, A. Zebda, E. Appert, C. Guiducci, M. Labeau, J.P. Diard, B.L. Gorrec, N. Brack, P.J. Pigram, Semiconductor oxide based electrodes for the label-free electrical detection of DNA hybridization: comparison between Sb doped SnO_2 and CdIn_2O_4 . *Electrochim. Acta* **51**(24), 5206–5214 (2006). <https://doi.org/10.1016/j.electacta.2006.03.045>
38. R. Al-Gaashani, S. Radiman, A.R. Daud, N. Tabet, Y. Al-Douri, XPS and optical studies of different morphologies of ZnO nanostructures prepared by microwave methods. *Ceram. Int.* **39**(3), 2283–2292 (2013). <https://doi.org/10.1016/j.ceramint.2012.08.075>
39. J. Das, S.K. Pradhan, D.R. Sahu, D.K. Mishra, S.N. Sarangi, B.B. Nayak, S. Verma, B.K. Roul, Micro-Raman and XPS studies of pure ZnO ceramics. *Phys. B* **405**(10), 2492–2497 (2010). <https://doi.org/10.1016/j.physb.2010.03.020>
40. J.H. Zheng, Q. Jiang, J.S. Lian, Synthesis and optical properties of flower-like ZnO nanorods by thermal evaporation method. *Appl. Surf. Sci.* **257**(11), 5083–5087 (2011). <https://doi.org/10.1016/j.apsusc.2011.01.025>
41. S. Karamat, R.S. Rawat, T.L. Tan, P. Lee, S.V. Springham, A. Rehman, R. Chen, H.D. Sun, Exciting diluted magnetic semiconductor: copper-doped ZnO. *J. Superconduct. Novel Magnet.* **26**(1), 187–195 (2013). <https://doi.org/10.1007/s10948-012-1710-2>
42. P. Luo, M. Xie, J. Luo, H. Kan, Q. Wei, Nitric oxide sensors using nanospiral ZnO thin film deposited by GLAD for application to exhaled human breath. *RSC Advances* **10**(25), 14877–14884 (2020). <https://doi.org/10.1039/d0ra00488j>
43. V.R. Shinde, T.P. Gujar, C.D. Lokhande, Enhanced response of porous ZnO nanobeads towards LPG: effect of Pd sensitization. *Sensors and Actuators B: Chemical* **123**(2), 701–706 (2007). <https://doi.org/10.1016/j.snb.2006.10.003>
44. P. Suchorska-Woźniak, O. Rac, M. Fiedot, H. Teterycz, Analysis of SnO_2/WO_3 heterocontact properties during the detection of hydrogen sulphide. *Sensors* **14**(11), 20480–20499 (2014). <https://doi.org/10.3390/s141120480>

Publisher's Note Springer Nature remains neutral with regard to jurisdictional claims in published maps and institutional affiliations.